Ceramics International xxx (xxxx) xxx

Contents lists available at ScienceDirect

Ceramics International

journal homepage: www.elsevier.com/locate/ceramint

Actual A-site Gd incorporation into $NdFeO_3$ perovskite lattice to induce transition in magnetic ordering for spintronic applications

T. Sindhu [a], M. Kumaresavanji [a], A. Robert Xavier [b], K. Sofiya [c], M. Baneto [d,e], K. Ravichandran [f], S. Ravi [a], A.T. Ravichandran [a,*]

[a] PG and Research Department of Physics, National College (Autonomous), Affiliated to Bharathidasan University, Tiruchirappalli, 620 001, Tamil Nadu, India
[b] Department of Physics, St. Joseph University, Nagaland, India
[c] Department of Chemical Engineering, SRM Institute of Science and Technology, Kattankulathur, Chennai, 603203, India
[d] Regional Centre of Excellence for Electricity Management (CERME), University of Lome, 01BP1515, Lome, Togo
[e] Department of Physics, University of Lomé, 01BP1515, Lomé, Togo
[f] PG & Research Department of Physics, AVVM Sri Pushpam College (Autonomous), (Affiliated to Bharathidasan University, Tiruchirappalli), Poondi, Thanjavur, 613 503, Tamil Nadu, India

ARTICLE INFO

Handling Editor: Dr P. Vincenzini

Keywords:
ABO_3
$NdFeO_3$
Solution combustion
Ferromagnetic
Spintronics

ABSTRACT

Here, we investigate the effect of structural and magnetic properties of Gadolinium (Gd) doped (x = 0, 0.05, and 0.1) Neodymium Iron Oxide ($NdFeO_3$) nanoparticles synthesized via slow solution combustion technique. The X-ray Diffraction (XRD) analysis confirmed an orthorhombic crystal structure with the space group Pbnm (JCPDS card no. 25–1149), and the crystallite size was found to decrease from 52 nm to 32 nm with increasing Gd doping concentration. Field Emission Scanning Electron Microscopy (FESEM) revealed well-organized and agglomerated nanoparticles with consistent particle sizes. Magnetic measurements were performed using SQUID magnetometer that demonstrated a ferromagnetic character for all samples, with an increase in magnetic moment as the Gd doping concentration increases. The hysteresis curves showed an increase in remanent magnetization and a decrease in coercivity from 0.7 T to 0.4 T. These findings suggest that Gd-doped $NdFeO_3$ nanoparticles, with their enhanced magnetic moments and reduced coercivity, hold potential for spintronic applications.

1. Introduction

In recent years, metal oxide (MO)-derived advanced materials have attracted significant scientific and technological interest due to their exceptional electrical, optical, mechanical, magnetic, and physical properties, making them suitable for a wide range of applications in material science, biomedicine, and chemistry [1–3]. Magnetic nanomaterials have been the focus of extensive research, both for their fundamental properties and their technological applications, including data storage, sensors, catalysts, magnetic resonance imaging, and biomedical uses [4–6]. Among these, ferrite materials, especially perovskite ferrites, have been widely studied and are recognized as excellent absorptive materials due to their remarkable absorption efficiency, tunability, and stability across a wide frequency range. Perovskite ferrites exhibit outstanding magnetic and dielectric properties, making them ideal for various applications such as electromagnetic shielding, wireless communication, and radar interference mitigation [7,8]. Furthermore, oxide materials are well-known for their remarkable characteristics, including high-temperature superconductivity, magnetoresistance, and multiferroicity, as well as their utility in devices like solid-oxide fuel cells, catalytic converters, and gas sensors [9,10].

Rare-earth ferrites ($RFeO_3$) exhibit a moderate dielectric constant, high magneto-crystalline anisotropy, and low magnetic permeability, making them highly suitable for fabrication of magnetic devices [8, 10–12]. Furthermore, RFeO3 perovskites demonstrate magnetically induced ferroelectric polarization which arises from the coupling between R^{3+} and Fe^{3+} ions. The domain walls in these materials display both ferroelectric and canted-antiferromagnetic properties with strong confinement, enabling the simultaneous control of electric polarization and magnetization through magnetic and electric fields [8,11]. This dual property of ferroelectricity and canted-antiferromagnetism in $RFeO_3$ compounds makes them highly versatile for advanced applications. The exceptional magnetoelectric properties of $RFeO_3$, such as reversible magnetic exchange bias, the magnetocaloric effect, and

* Corresponding author. National College Autonomous, Tiruchirappalli, 620001, India.
E-mail address: atrnct@gmail.com (A.T. Ravichandran).

https://doi.org/10.1016/j.ceramint.2025.01.262
Received 21 November 2024; Received in revised form 20 December 2024; Accepted 13 January 2025
Available online 17 January 2025

magnetism-driven ferroelectricity, have garnered considerable interest in materials research. Nano-sized ferrites, in particular, possess a higher specific surface area compared to their bulk counterparts due to the quantum size effect. This increased surface area enables the incorporation of various dopants into their structure, allowing the properties to be tailored based on the type of dopant material used. Additionally, the preferential occupation of A-sites or B-sites by the dopant elements can significantly influence the electrical, optical, and magnetic properties of RFeO3 [13–15].

Particularly, the orthorhombic symmetry of the Neodymium Iron oxide ($NdFeO_3$) perovskites exhibited interesting magnetic interactions such as Nd–Nd, Nd–Fe, and Fe–Fe. In this transition, the direction of the easy axis of magnetization changes from one crystal axis to another induced by temperature or applied field [16,17]. $NdFeO_3$ is a type of Perovskite oxide that is ferromagnetic and its magnetic properties mainly depend on the interaction between Nd^{3+}-Fe^{3+}, Fe^{3+}-Fe^{3+}, and Nd^{3+}-Nd^{3+}. For instance, Abida Bashir et al. [18] examined and reported the change in magnetic behaviour by the addition of Ni^{3+} which replaces Fe site causing a spin reorientation of Fe^{3+} and new magnetic interaction when doped with $NdFeO_3$.

In terms of its structure, $NdFeO_3$ displays a distorted orthorhombic configuration within the *Pbnm* space group, with each unit cell containing four formula units [19]. This distortion notably alters the intensity of super exchange interactions, with the interplay between magnetic ions ($Nd^{3+}$and Fe^{3+}) influenced by temperature variations. In this transition, the orientation of the magnetic axis shifts from one crystal axis to another due to temperature variations or an applied magnetic field. An extensive examination of spin reorientation, structure change and the underlying mechanism of spin reorientation within $NdFeO_3$ were done by Slawinski et al. [20] and L. Chen et al. [21], respectively. Although $NdFeO_3$ has been thoroughly investigated at low temperatures, there is limited literature available regarding its properties at higher temperatures, particularly close to the Néel temperatures.

Synthesis of $RFeO_3$ nano ferrites through solution combustion technique with nitrate precursors and fuels, often faces challenges such as non-uniform atomic stoichiometric ratios and the emergence of undesired phases [22–24]. In recent years, there has been a surge in attempts to produce these compounds through diverse methods like sol-gel, for improved regulation of particle size. It has been noted that there are changes in the physical attributes, including the magnetic and dielectric properties. In this paper, the structural, surface morphological and magnetic characteristics of Gd doped $NdFeO_3$ synthesized using the solution combustion method were systematically investigated. The magnetic parameters such as Curie temperature, saturation magnetization and remanent magnetization were determined and analysed from temperature and field dependence of magnetization measurements.

2. Experimental method

The undoped and Gd doped $NdFeO_3$ nanomaterials were synthesized by solution combustion method using citric acid as fuel. The $Nd(NO_3)_3{\cdot}6H_2O$ (99.9 %), $Fe(NO_3)_3{\cdot}9H_2O$ (99.0 %) and $Gd(NO_3)_3.6H_2O$ (99.9 %) were taken as precursors to synthesize the $Nd_{1-x}Gd_xFeO_3$ (x = 0, 0.05 and 0.1) nanoparticles. All initial chemical components were carefully measured for the preparation of various samples. Each compound was dissolved in deionized water in the necessary quantities to create a 1 M solution individually. Subsequently, the amalgamation of nitrates and citric acid was transferred into a beaker and stirred with a magnetic stirrer to ensure uniformity in the solution. The solution began to heat up, reaching a boiling point, and eventually underwent a self-propagating ignition process, resulting in complete combustion, after being continuously heated to approximately 200 °C. The resultant was an ash powder. The nanocrystalline powder was obtained by grinding the ash powder and calcining it at 700 °C for 5 h. The final product was powdered and then investigated. Fig. 1 illustrates the pictorial representation of preparation procedure of $Nd_{1-x}Gd_xFeO_3$ (x = 0, 0.05 and 0.1) nanoparticles.

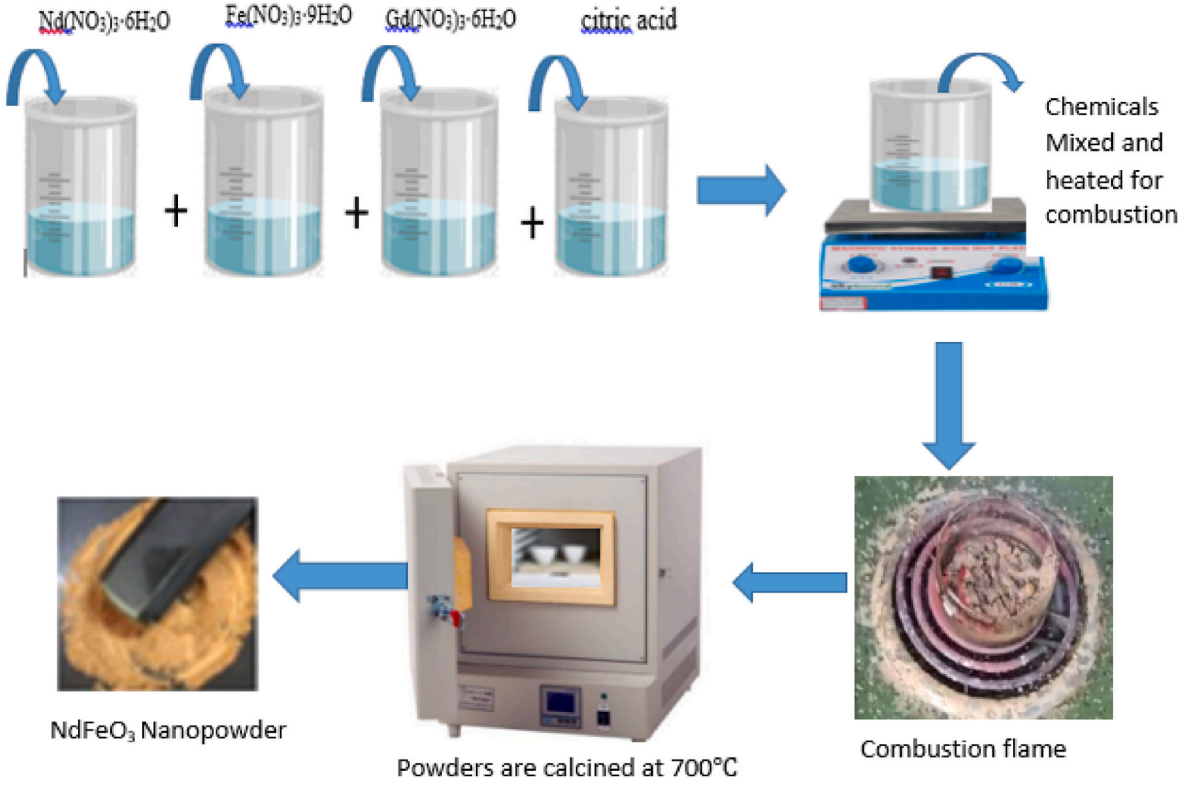

Fig. 1. Pictorial representation of the synthesis of Gd doped $NdFeO_3$ nanoparticles.

3. Results and discussion

3.1. Structural analysis

All the prepared nanoparticles were examined by powder X-ray diffraction (XRD) using X'PERT-PRO X-ray diffractometer. Fig. 2 shows the XRD patterns of undoped and Gd doped $NdFeO_3$ nanoparticles calcined at 700 °C. The X-ray diffraction pattern of $NdFeO_3$ closely resembles that of the orthorhombic crystal structure, especially within the space group *Pbnm* [25]. The obtained patterns also indicate high level of purity as there are no secondary phases found. This is confirmed by indexing the diffraction peaks using JCPDS pattern no. 25–1149 which offers confirmation in support of the claim [26]. The widening observed in the X-ray diffraction peaks suggests a reduction in the size of nanoparticles. The Scherrer equation has been utilized to determine the precise dimensions of the crystallites. The average crystallite size (L) of the ferrite samples can be accomplished by correlating it with the most prominent peak (121) and the FWHM (β) of the XRD peak as given by the Debye-Scherrer's [27] equation:

$$L = k\lambda/\beta \cos\theta \quad (1)$$

where the Scherrer constant k, the wavelength of X-ray λ and the Bragg's peak radian angle θ are the main parameters of this analysis approximately. The crystallite size is decreased from 52 to 32 nm with increase in the Gd doping concentration. It is also known that the crystallite size value obtained from the Debye-Scherrer formula may not be entirely precise. Hence, an established relationship devised by Williamson and Hall (W–H) plot is employed. This graph enables the differentiation between micro-strain input and the broadening of the XRD peak, providing more customized measurements regarding the crystallite size. The complete FWHM of the XRD peak is correlated with the sample's crystallite size (L) and micro-strain (ε) [28] as represented by the equation,

$$\beta \cos\theta = \frac{k\lambda}{L} + 4\varepsilon \sin\theta \quad (2)$$

The symbols used in the analysis are defined by equation (1). Additionally, the intercept kλ/L is utilized to estimate the size of the crystallites.

A crystallite size of 33.58 nm was obtained for the $NdFeO_3$ sample.

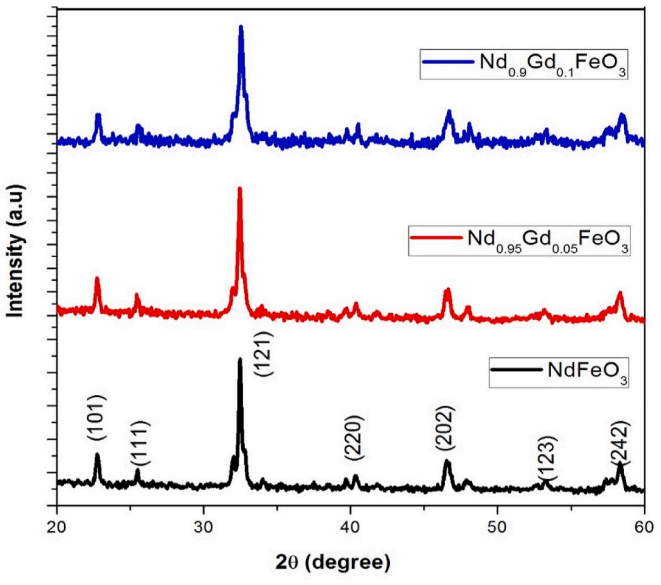

Fig. 2. X-ray diffraction patterns of undoped and Gd (x = 0, 0.05 and 0.1) doped $NdFeO_3$.

Notably, the estimated crystallite size has been found to be greater than Debye Scherrer's value. This observation is attributable to the fact that the crystallite size has an inverse relationship to the FWHM of the XRD peak and that the presence of micro-strain results in a lower FWHM. As a result, a higher value of crystallites is obtained. The positive sign of the induced strain in the nanoparticle suggests a distorted crystal structure due to Oxygen vacancy and interfacial imperfection. With the increase in Gd concentration, the XRD peak is found to be shifted towards a higher 2θ (right shift) indicating a slight decrease in interplanar distance caused by the smaller ionic radius of the dopant (0.94 Å) compared with that of the host ion (1.12 Å). It is also noticed that the peak width is gradually broadened while the intensity of the peaks decreases. This broadening of the peaks indicates the decrease in the crystallite size and unit cell volume. Such a decrease is also a confirmation for the Gd (III) substitution to Nd (III) in the $NdFeO_3$ crystal lattice.

3.2. Surface morphology and elemental analysis

In order to investigate the morphology of the $Nd_{1-x}Gd_xFeO_3$ nanoparticles, a Field Emission Scanning Electron Microscope (FESEM) was employed using ZEISS ultra plus with 20 kV FESEM. It is preferred for such analysis due to its straightforward image interpretation and simple sample preparation procedures. Fig. 3(a–c) shows the FESEM images of undoped and Gd doped $NdFeO_3$. These images illustrate the uneven form of the grains, primarily spherical with a slight inclination to clump together. However, the magnification confirms that the grains comprise exceedingly fine particles.

In order to identify the constituent elements present in the sample, Energy Dispersive X-ray spectroscopy (EDX) was conducted, and the obtained results are presented in Fig. 4. Specifically, the spectra confirm the signature of Nd, Fe in the material as well as Gd present in the doped sample. But the oxygen (O) peak is not visible due to its low energy emission (around 0.5 keV) and potential masking by background noise or equipment limitations.

3.3. High-resolution transmission electron microscopy (HRTEM)

High Resolution Transmission Electron Microscopy (HRTEM) for the as prepared nanoparticles were carried out using JEOL Japan, JEM-2100 Plus. Fig. 5a shows the morphology and structure of the undoped $NdFeO_3$ nanoparticles. As can be seen, the shape of the particles of the synthesized $NdFeO_3$ samples is close to spherical, but agglomerates of particles are noticeable. The particles appear smaller and more uniform compared to the doped version, indicating a different aggregation or growth behaviour. Fig. 5a (b) shows the selected area electron diffraction (SAED) pattern, indicating the crystalline structure, with diffraction spots suggesting a well-ordered crystalline nature. The lattice fringes seen in Fig. 5a (c) are clear, indicating good crystallinity.

Fig. 5b (d) shows aggregated clusters with an irregular shape of $Nd_{0.95}Gd_{0.05}FeO_3$ nanoparticles. The particles appear somewhat larger and more irregular compared to the undoped sample. Fig. 5b (e) (Selected Area Electron Diffraction, SAED Patterns) shows a crystalline structure with distinct diffraction spots. The pattern indicates a well-ordered crystal structure, possibly with some distortion due to Gd doping. Fig. 5b (f) shows visible lattice fringes, indicating the crystalline nature of the $Nd_{0.95}Gd_{0.05}FeO_3$ material. The lattice appears ordered, however shows minor distortions due to the presence of Gd atoms.

Fig. 5c (g) shows elongated, irregular cluster of grains of $Nd_{0.9}Gd_{0.1}FeO_3$. The particles appear larger and more aggregated than the 5 at % doped and undoped samples, indicating that the increased Gd doping affects the particle morphology. The SAED pattern displays a crystalline structure with diffraction spots. The spots are less sharp or more diffuse compared to the 5 at % doped and undoped samples, indicating increased lattice distortions or strain due to higher Gd doping. The HRTEM lattice fringe image shows lattice fringes, but they are less uniform compared to the 5 at % doped and undoped samples. The higher

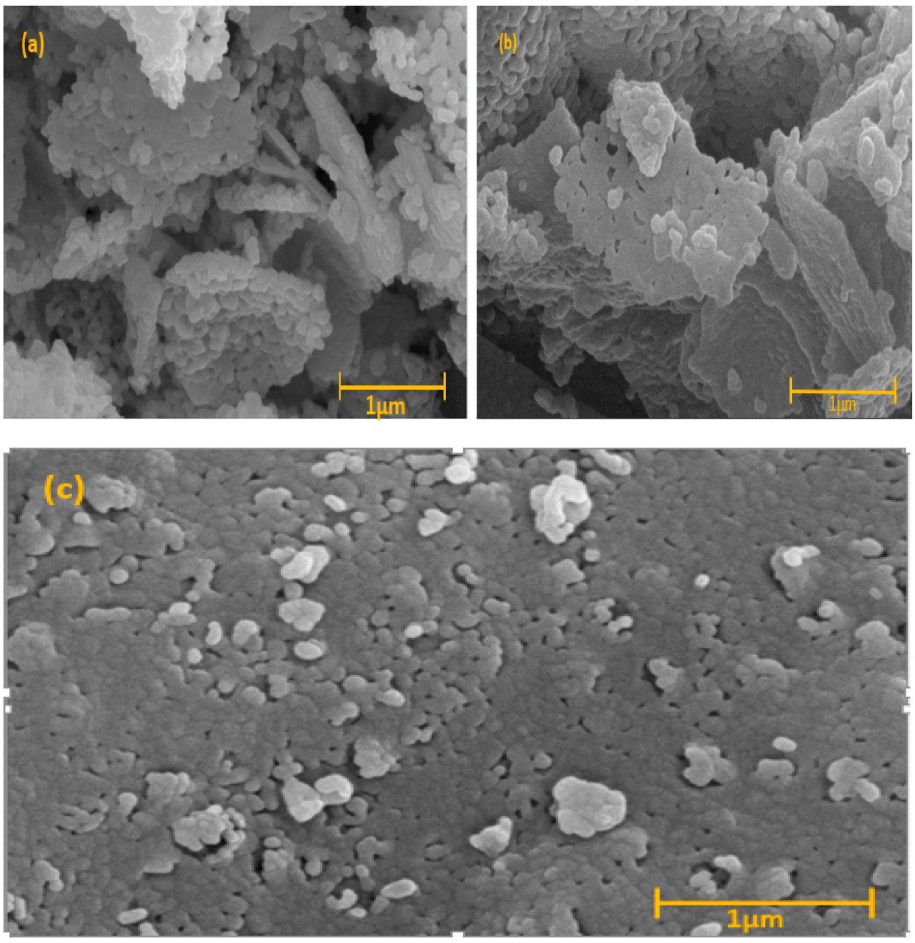

Fig. 3. FESEM images of (a) $NdFeO_3$ (b) $Nd_{0.95}Gd_{0.05}FeO_3$ (c) $Nd_{0.9}Gd_{0.1}FeO_3$ nanoparticles calcined at 700 °C.

Gd doping level could introduce more significant distortions or defects in the crystal lattice. An analysis of the results of the size distribution of Gd doped $NdFeO_3$ grains allows us to conclude that the average grain size decreases monotonically with an increase in the dopant content in the synthesized samples. In the undoped $NdFeO_3$ sample, clear lattice fringes are observed, indicating high crystallinity. However, in the Gd-doped sample, changes in the spacing or regularity of these fringes suggest that Gd doping affects the crystal structure, leading to lattice distortions or reduced crystallinity. Changes in lattice structure and crystallinity can alter the magnetic properties of $NdFeO_3$, making Gd-doped variants useful in designing magnetic sensors, memory devices, and spintronic applications.

3.4. Magnetic studies

The temperature and field dependence of magnetization were measured for $Nd_{1-x}Gd_xFeO_3$ nanoparticles by using SQUID magnetometer. The temperature-dependent magnetization measurements were performed under both field-cooled (FC) and zero-field-cooled (ZFC) conditions, using an applied magnetic field of 100 Oe. Additionally, the field-dependent magnetization was measured at 5 K and 300 K, with the applied magnetic field ranging up to 5 T. Fig. 6 exhibits the magnetic behaviour of all the samples with respect to temperature. From the measurements, it is clear to observe a ferromagnetic to paramagnetic transition for all the samples. At 5 K, all samples exhibit ferromagnetic behaviour, as indicated by the upward bending of the curves with decreasing temperature. This upward trend signifies that as the magnetic field strength increases, the magnetic moments align more effectively, leading to greater overall magnetization. Ferromagnetic materials naturally possess a net magnetization even in the absence of an external magnetic field, due to the alignment of magnetic moments within the material. Doping does not eliminate ferromagnetism but can modify its strength or other magnetic properties depending on the material's composition. The Curie temperature (T_C) for the undoped nanoparticles is approximately 13 K, rising to 34 K for $Nd_{0.9}Gd_{0.1}FeO_3$. Consequently, the paramagnetic behaviour decreases as the Gd doping concentration increases. The enhancement in ferromagnetism is a complex phenomenon governed by factors such as the material's crystal structure and the magnetic interactions among its elements [29,30].

Fig. 7 demonstrates the field dependence of magnetization curves for all samples measured at 5K. As seen in the curves, the decrease in the slope of the magnetization response indicates a reduction in paramagnetic behaviour and an increase in ferromagnetic behaviour, consistent with the addition of Gd dopant. The observed increase in the magnitude of the magnetic response with increasing Gd dopant content supports the notion of enhanced ferromagnetic behaviour. The saturation magnetization observed for higher doping confirms that the Gd dopant favours the ferromagnetic behaviour in $NdFeO_3$ and supports the results obtained from temperature dependence of magnetization (Fig. 6).

The same hysteresis curves were obtained for 300 K which is illustrated in Fig. 8. It is observed that the magnetic curves do not saturate even for high doping concentration of Gd. However, the MH curves exhibit a large coercivity (H_C) and exhibit a similar tendency as the Gd content increases. Fig. 9 demonstrate the variation of H_C and remanent magnetization (M_r) with respect to Gd dopant concentration. As the Gd content increases, the M_r also increases and indicate the aptness of Gd to improve the magnetic ordering state in $NdFeO_3$. Meanwhile, the

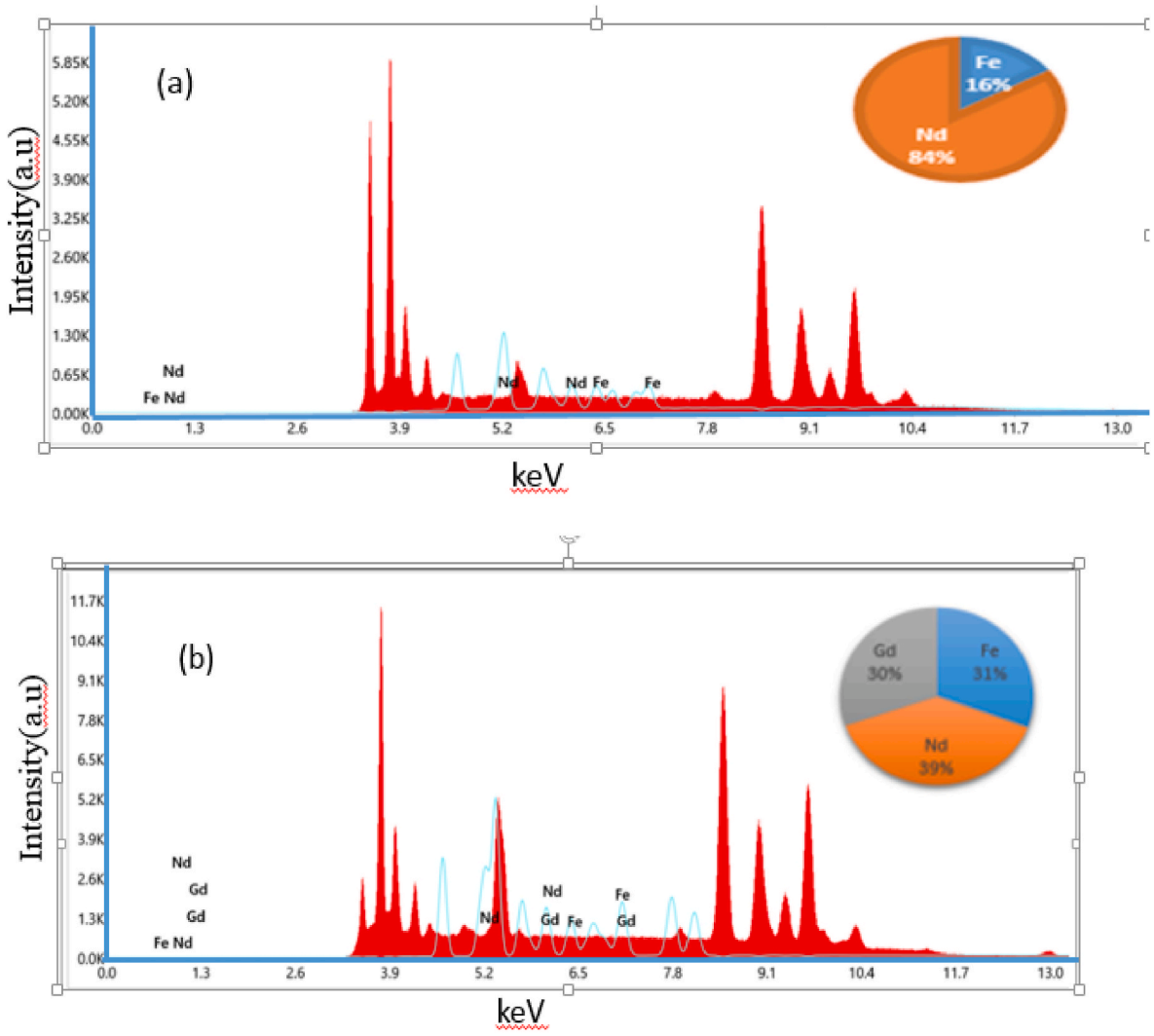

Fig. 4. EDX spectra of (a) $NdFeO_3$ and (b) $Nd_{0.9}Gd_{0.1}FeO_3$ nanoparticles.

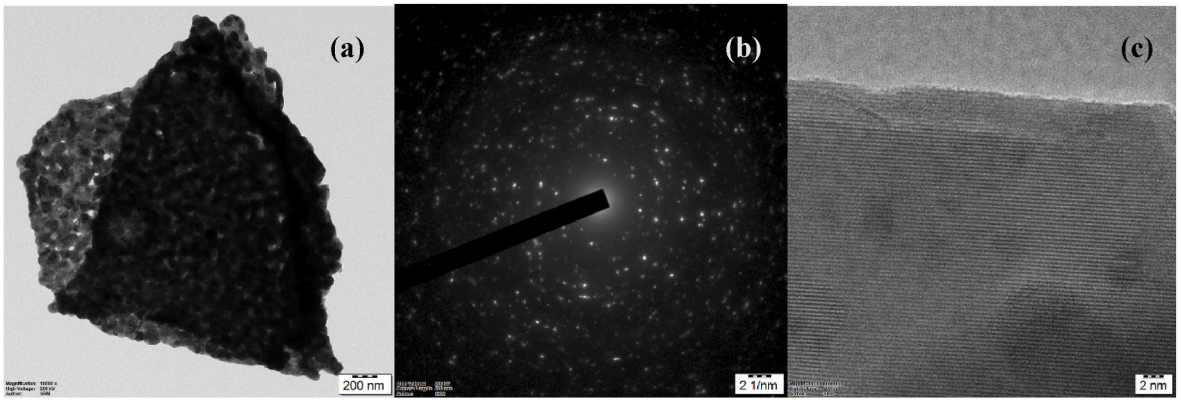

Fig. 5a. HRTEM images of $NdFeO_3$ at (a)200 nm, (b)21 nm and (c)2 nm.

coercivity decreases sharply with the dopant of Gd that shows the soft magnetic nature of $NdFeO_3$ with Gd.

In consequence, doping Gd into $NdFeO_3$ enhances its magnetic properties by introducing Gd^{3+} ions with a higher magnetic moment (7 μ_B) compared to Nd^{3+}. This substitution can strengthen the exchange interactions between the Fe^{3+} ions and the rare-earth ions and hence promote ferromagnetic ordering. Moreover, Gd doping can modify the crystal structure, leading to changes in bond angles and bond lengths, which influence the magnetic exchange pathways. These results could be valuable for tailoring magnetic properties in ferrite materials and highlights the intricate nature of magnetic materials and their response to changes in composition. Moreover, understanding the relationship between Gd content and magnetization parameters like H_C and Mr is crucial in designing magnetic materials for various applications.

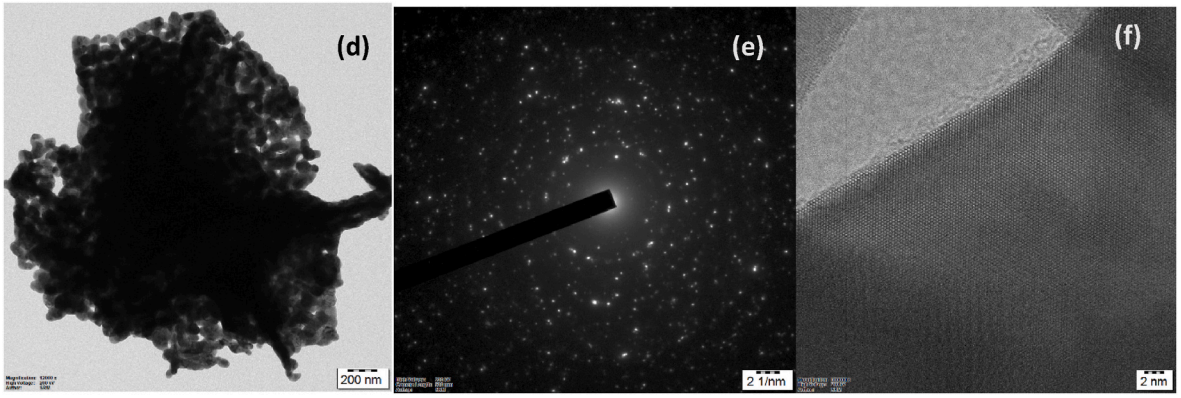

Fig. 5b. HRTEM images of $NdFeO_3$ doped with 5 at% gadolinium at (d)200 nm (e)21 nm (f)2 nm.

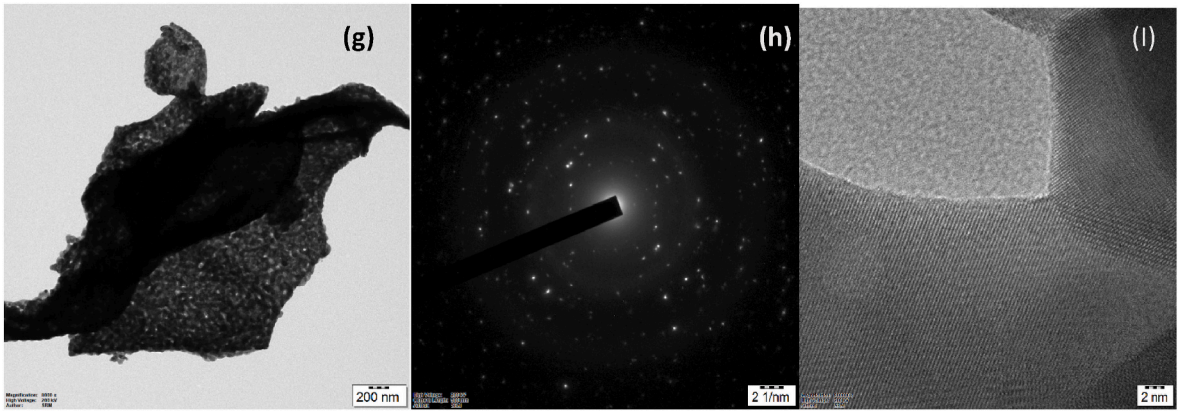

Fig. 5c. HRTEM images of $NdFeO_3$ doped with 10 at% gadoliniumat (g)200 nm, (h)21 nm, (i)2 nm.

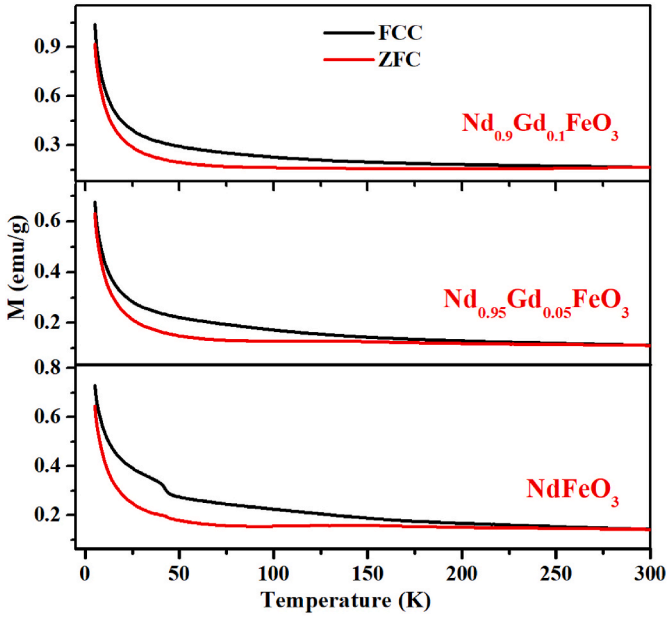

Fig. 6. Temperature dependent Magnetization for $Nd_{1-x}Gd_xFeO_3$ (x = 0, 0.05 and 0.1) under FC and ZFC conditions.

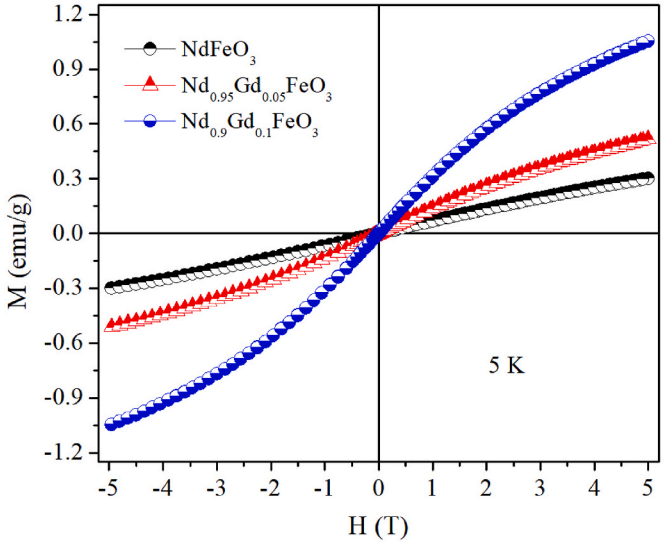

Fig. 7. Hysteresis loops measured at 5 K for $Nd_{1-x}Gd_xFeO_3$ (x = 0, 0.05 and 0.1).

4. Conclusion

The $Nd_{1-x}Gd_xFeO_3$ (x = 0, 0.05 and 0.1) was effectively synthesized by solution combustion method. The XRD analysis confirmed the orthorhombic structure with space group Pbnm. The average crystallite size was found to be reduced from 55 to 32 nm as the Gd doping

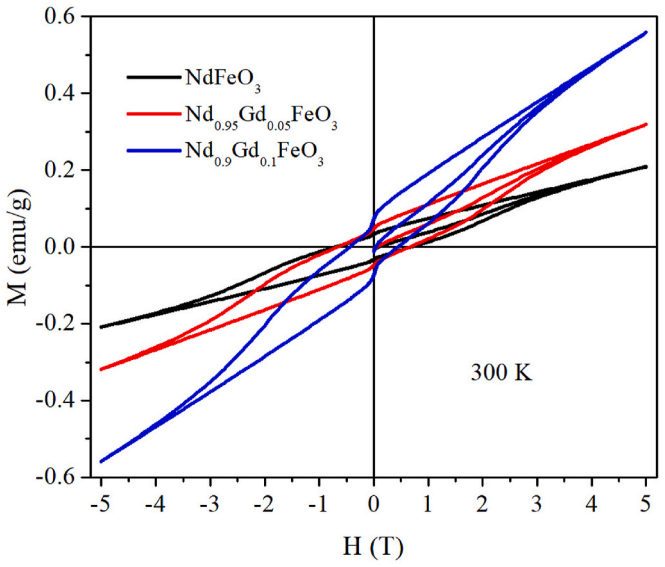

Fig. 8. Hysteresis loops of undoped and Gd doped $NdFeO_3$ nanoparticles measured at 300 K.

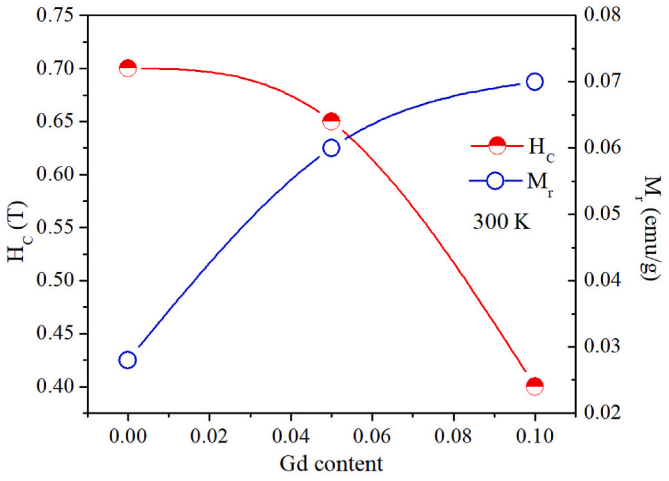

Fig. 9. Change in H_C and M_r with respect to Gd dopant concentration.

concentration increases to 0.1. The FESEM images depict uneven grains but they are found to be spherical in shape. The EDX spectra confirm the presence of Nd, Gd, Fe, and absence of O due to low energy emission in the synthesized samples. As per HRTEM analysis, Gd doping affects the morphology, crystallinity, and lattice structure of $NdFeO_3$. The magnetic property reveals its response to changes in composition and the H_C starts from 0.7 T and decreases to 0.4 T. These properties influence the performance and efficiency of devices and systems utilizing magnetic materials, and optimizing them can lead to improved functionality and reliability of devices such as magnetic recording media, magnetic sensors, and magnetic nanoparticles for biomedical applications.

CRediT authorship contribution statement

T. Sindhu: Writing – original draft, Visualization, Software, Resources, Methodology, Investigation, Formal analysis, Data curation. **M. Kumaresavanji:** Writing – review & editing, Supervision, Project administration, Investigation, Funding acquisition, Conceptualization. **A. Robert Xavier:** Writing – review & editing, Writing – original draft, Visualization, Validation, Supervision, Methodology, Investigation. **K. Sofiya:** Resources, Formal analysis, Data curation. **M. Baneto:** Writing – review & editing, Supervision, Investigation. **K. Ravichandran:** Writing – review & editing, Visualization, Supervision, Data curation. **S. Ravi:** Writing – review & editing, Supervision, Resources. **A.T. Ravichandran:** Supervision, Project administration, Investigation, Formal analysis, Conceptualization.

Data availability statement

All data that support the findings of this study are included within the article.

Declaration of competing interest

The authors declare that they have no known competing financial interests or personal relationships that could have appeared to influence the work reported in this paper.

Acknowledgments

M Kumaresavanji acknowledges DST-SERB, India for the financial support through SERB-TARE project (TAR/2019/000463).

References

[1] M.S. Chavali, M.P. Nikolova, Metal oxide nanoparticles and their applications in nanotechnology, SN Appl. Sci. 1 (2019) 607, https://doi.org/10.1007/s42452-019-0592-3.
[2] P. Deva, S. Ravi, E. Manikandan, Facile synthesis of CuMn2O4 nanoparticles for efficient of high-performance electrode materials for supercapacitor application, Ceram. Int. 50 (2014) 11916–11927, https://doi.org/10.1016/j.ceramint.2024.01.095.
[3] U. Farooq, T. Ahmad, F. Naaz, S. ul Islam, Review on metals and metal oxides in sustainable energy production: progress and perspectives, Energy Fuels 37 (2023) 1577–1632, https://doi.org/10.1021/acs.energyfuels.2c03396.
[4] A.H. Shah, M.B. Ahamed, E. Manikandan, R. Chandramohan, M. Iydroose, Magnetic, optical and structural studies on Ag doped ZnO nanoparticles, J. Mater. Sci. Mater. Electron. 24 (2013) 2302–2308, https://doi.org/10.1007/s10854-013-1093-6.
[5] A. Diallo, T. Doyle, B. Mothudi, E. Manikandan, V. Rajendran, M. Maaza, Magnetic behaviour of biosynthesized Co3O4 nanoparticles, J. Magn. Magn Mater. 424 (2017) 251–255, https://doi.org/10.1016/j.jmmm.2016.10.063.
[6] R. Bushra, M. Ahmad, K. Alam, F. Seidi, Qurtulen, Sadaf Shakeel, J. Song, Y. Jin, H. Xiao, Recent advances in magnetic nanoparticles: key applications, environmental insights, and future strategies, Sustain. Mater. Technol. 40 (2024) e00985, https://doi.org/10.1016/j.susmat.2024.e00985.
[7] Anna Paola Panunzi, Leonardo Duranti, Umer Draz, Silvia Licoccia, Cadia Dottavi, Elisabetta Di Bartolomeo, Improved surface activity of lanthanum ferrite perovskite oxide through controlled Pt-doping for solid oxide cell (SOC) electrodes, Ceram. Int. 50 (2024) 31442–31450, https://doi.org/10.1016/j.ceramint.2024.05.451.
[8] R. Vilarinho, M.C. Weber, M. Guennou, A.C. Miranda, C. Dias, P. Tavares, J. Kreisel, A. Almeida, J. Agostinho Moreira, Magneto structural coupling in RFeO3 (R = Nd, Tb, Eu and Gd), Sci. Rep. 12 (2022) 1–15, https://doi.org/10.1038/s41598-022-13097-1.
[9] S. Ning, A. Kumar, K. Klyukin, E. Cho, J.H. Kim, T. Su, H.S. Kim, J.M. LeBeau, B. Yildiz, C.A. Ross, An antisite defect mechanism for room temperature ferroelectricity in orthoferrites, Nat. Commun. 12 (2021) 4298, https://doi.org/10.1038/s41467-021-24592-w.
[10] N. Aparnadevi, K. Saravana Kumar, M. Manikandan, D.P. Joseph, C. Venkateswaran, Room Temperature dual ferroic behaviour of ball mill synthesized NdFeO3 orthoferrites, J. Appl. Phys. 120 (2016) 04101, https://doi.org/10.1063/1.4954842.
[11] Z.X. Cheng, F. Hong, Y.X. Wang, K. Ozawa, H. Fujii, Interface strain induced multiferroicity in a SmFeO3 film, ACS Appl. Mater. Interfaces 6 (2014) 7356–7362, https://doi.org/10.1021/am500762c.
[12] Y. Tokunaga, S. Iguchi, T. Arima, Y. Tokura, Magnetic-field induced ferroelectric state in DyFeO3, Phys. Rev. Lett. 101 (2008) 097205, https://doi.org/10.1103/PhysRevLett.101.097205.
[13] M. Das, S. Roy, P. Mandal, Giant reversible magnetocaloric effect in a multiferroic GdFeO3 single crystal, Phys. Rev. 96 (2017) 174405.
[14] Z.Q. Wang, Y.S. Lan, Z.Y. Zeng, X.R. Chen, Q.F. Chen, Magnetic structures and RSC optical properties of rare-earth orthoferrites RFeO3 (R = Ho, Er, Tm and Lu), Solid State Commun. 288 (2019) 10–17.
[15] C. Sasikala, N. Durairaj, I. Baskaran, B. Sathyaseelan, M. Henini, E. Manikandan, Transition metal titanium (Ti) doped LaFeO3 nanoparticles for enhanced optical structural and magnetic properties, J. Alloys Compd. 712 (2017) 870–877, https://doi.org/10.1016/j.jallcom.2017.04.133.
[16] R. Przenioslo, I. Sosnowska, P. Fischer, Magnetic moment ordering of Nd3+ions in NdFeO3, J. Magn. Magn Mater. 140–144 (1995) 2153–2154.

[17] T. Shalini, P. Vijayakumar, J. Kumar, Studies on structural and magnetic properties of NdFeO3 single crystals grown by optical floating zone technique, Bull. Mater. Sci. 43 (2020) 285, https://doi.org/10.1007/s12034-020-02259-4.
[18] A. Bashir, M. Ikram, R. Kumar, P. Thakur, K.H. Chae, W.K. Choi, V.R. Reddy, Structural, magnetic and electronic structure studies of NdFe1- xNixO3 (0≤x≤0.3), J. Phys. Condens. Matter 21 (32) (2009) 325501.
[19] J. Ramesh, N. Raju, S.S.K. Reddy, M. Sreenath Reddy, Ch Gopal Reddy, P. Yadagiri Reddy, K. Rama Reddy, V. Raghavendra Reddy, 57Fe Mossbauer study of spin reorientation transition in polycrystalline NdFeO3, J. Alloys Compd. 711 (2017) 300–304.
[20] W. Slawinski, R. Przeniosło, I. Sosnowska, E. Suard, Spin reorientation and structural changes in NdFeO3, J. Phys. Condens. Matter 17 (2005) 4605–4614.
[21] L. Chen, T. Li, S. Cao, S. Yuan, F. Hong, J. Zhang, The role of 4f-electron on spin reorientation transition of NdFeO3: a first principle study, Phys. Rev. B 111 (2012) 103905.
[22] M. Khorasani Motlagh, M. Noroozifar, M. Yousefi, Sh Jahani, Chemical synthesis and characterization of perovskite NdFeO3nanocrystals via a co-precipitation method, Int. J. Nanosci. Nanotechnol. 9 (1) (March 2013).
[23] A. Wu, H. Shen, J. Xu, L. Jiang, L. Luo, S. Yuan, S. Cao, H. Zhang, Preparation and magnetic properties of RFeO3 nanocrystalline powders, J. Sol. Gel Sci. Technol. 59 (2011) 158–163.
[24] T. Sindhu, A.T. Ravichandran, A. Robert Xavier, M. Kumaresavanji, Structural, surface morphological and magnetic properties of Gd-doped BiFeO3 nanomaterials synthesised by EA chelated solution combustion method, Appl. Phys. A 129 (2023) 685, https://doi.org/10.1007/s00339-023-06951-0.
[25] A. Somvanshi, A. Ahmad, S. Husain, S. Manzoor, Aref A.A. Qahtan, N. Zarrin, M. Fatema, W. Khan, Structural modifications and enhanced ferroelectric nature of NdFeO3–PbTiO3 composites, Appl. Phys. A 127 (2021) 424, https://doi.org/10.1007/s00339-021-04562-1.
[26] Y. Wang, S. Cao, M. Shao, S. Yuan, B. Kang, B. Zhang, A. Wu, J. Xu, Growth rate dependence of the NdFeO3 single crystal grown by float-zone technique, J. Cryst. Growth 318 (2011) 927–931, https://doi.org/10.1016/j.jcrysgro.2010.11.020.
[27] Y.A. O Bokuniaeva, A.S. Vorokh, Estimation of particle size using the Debye equation and the Scherrer formula for polyphasic TiO2 powder, J. Phys.: Conf. Ser. 1410 (2019) 012057, https://doi.org/10.1088/1742-6596/1410/1/012057.
[28] A. B Hariyanto, D.A.P. Wardani, N. Kurniawati, N.P. Har, N darmawan and irzaman, X-ray peak profile analysis of silica by Williamson–Hall and size-strain plot methods, J. Phys.: Conf. Ser. 2019 (2021) 012106, https://doi.org/10.1088/1742-6596/2019/1/012106.
[29] T. Sindhu, A.T. Ravichandran, A. Robert Xavier, K. Sofiya, M. Kumaresavanji, Impact of Gd doping on structural and magnetic characteristics of SrFeO3 perovskite nanomaterial, J. Phys. Condens. Matter 36 (2024) 505809, https://doi.org/10.1088/1361-648x/ad7b94.
[30] C. Kumaran, I. Baskaran, B. Sathyaseelan, K. Senthilnathan, E. Manikandan, Effect of doping of iron on structural, optical and magnetic properties of CeO2 nanoparticles, Chem. Phys. Lett. 808 (2022) 140110, https://doi.org/10.1016/j.cplett.2022.140110.